NIH Public Access
Author Manuscript
Ultrasonics. Author manuscript; available in PMC 2014 September 01.

Published in final edited form as:
Ultrasonics. 2013 September ; 53(7): 1384–1391. doi:10.1016/j.ultras.2013.04.007.

Correlation of ultrasound contrast agent derived blood flow parameters with immunohistochemical angiogenesis markers in murine xenograft tumor models

John R. Eisenbrey[1], **Christian C. Wilson**[1,2], **Raymond J. Ro**[1,3], **Traci B Fox**[4], **Ji-Bin Liu**[1], **See-Ying Chiou**[1], and **Flemming Forsberg**[1]

[1]Department of Radiology, Thomas Jefferson University, Philadelphia, PA 19107

[2]College of Physicians and Surgeons, Columbia University, New York, NY 10032

[3]School of Biomedical Engineering, Sciences and Health Systems, Drexel University, Philadelphia, PA19104

[4]Department of Radiological Sciences, Jefferson School of Health Professions, Thomas Jefferson University, Philadelphia, PA19107

Abstract

Purpose—In this study we used temporal analysis of ultrasound contrast agent (UCA) wash-in to estimate blood flow dynamics and demonstrate their improved correlation to angiogenesis markers relative to previously reported, non-temporal fractional vascularity estimates.

Materials and Methods—Breast tumor (NMU) or glioma (C6) cells were implanted in either the abdomen or thigh of 144 rats. After 6, 8 or 10 days, rats received a bolus UCA injection of Optison (GE Healthcare, Princeton, NJ; 0.4ml/kg) during power Doppler imaging (PDI), harmonic imaging (HI), and microflow imaging (MFI) using an Aplio ultrasound scanner with 7.5 MHz linear array (Toshiba America Medical Systems, Tustin, CA). Time-intensity curves of contrast wash-in were constructed on a pixel-by-pixel basis and averaged to calculate maximum intensity, time to peak, perfusion, and time integrated intensity (TII). Tumors were then stained for 4 immunohistochemical markers (bFGF, CD31, COX-2, and VEGF). Correlations between temporal parameters and the angiogenesis markers were investigated for each imaging mode. Effects of tumor model and implant location on these correlations were also investigated.

Results—Significant correlation over the entire dataset was only observed between TII and VEGF for all three imaging modes ($R=-0.35,-0.54,-0.32$ for PDI, HI and MFI, respectively; $p<0.0001$). Tumor type and location affected these correlations, with the strongest correlation of TII to VEGF found to be with implanted C6 cells ($R=-0.43,-0.54,-0.52$ for PDI, HI and MFI, respectively; $p<0.0002$).

Conclusions—While UCA-derived temporal blood flow parameters were found to correlate strongly with VEGF expression, these correlations were also found to be influenced by both tumor type and implant location.

© 2013 Elsevier B.V. All rights reserved.

Corresponding Author: Flemming Forsberg, Department of Radiology, Thomas Jefferson University, 132 South 10th Street, Philadelphia, PA19107, USA, tel: 215-955-4870, fax: 215-955-8549, flemming.forsberg@jefferson.edu.

Publisher's Disclaimer: This is a PDF file of an unedited manuscript that has been accepted for publication. As a service to our customers we are providing this early version of the manuscript. The manuscript will undergo copyediting, typesetting, and review of the resulting proof before it is published in its final citable form. Please note that during the production process errors may be discovered which could affect the content, and all legal disclaimers that apply to the journal pertain.

NIH-PA Author Manuscript
NIH-PA Author Manuscript
NIH-PA Author Manuscript

NIH-PA Author Manuscript

NIH-PA Author Manuscript

NIH-PA Author Manuscript

Keywords

ultrasound contrast agents; angiogenesis; parametric imaging; immunohistochemical markers

1. Introduction

Ultrasound contrast agents (UCA; for list of abbreviations see appendix 1) are gas filled microbubbles encapsulated by an outer shell (generally of polymer or lipid) for stability. These agents provide ultrasound contrast due to differences in the compressibility and impedance of the gas core relative to the surrounding medium [1]. These agents act as excellent blood pooling agents due to their size (1–6 μm), which makes them too large to extravasate out of the blood stream, but small enough to transverse the capillary bed [1,2]. The ability to track the perfusion of these agents in real time has also been shown to be useful for the quantification of blood flow dynamics in a variety of applications [3–5].

Contrast-enhanced ultrasound (CEUS) has been used extensively in the imaging of angiogenesis [6–13]. The ability to visualize the tortuous neovasculature within a tumor using CEUS allows for improved identification of cancer [8–10], while changes in this vascularity have also shown to be a useful indicator of treatment response [9,10]. This power of detection appears to increase when using dynamic-CEUS [8,13]. Due to the real time nature of ultrasound and the blood pooling properties of UCA, visualization of UCA perfusion provides an indicator of the blood flow kinetics within the area of interest. Parameters such as the time required from injection to contrast arrival, rate of UCA inflow, rate of UCA washout, and cumulative UCA signal over time (an indicator of net blood flow) have all been shown to be potentially useful indicators of lesion malignancy or response to treatment [8,13], and packages to quantify these parameters are now commercially available. Additionally, this analysis can be performed on a pixel-by pixel basis to create parametric maps. These maps illustrate differences in blood flow kinetics within a given region of interest (which are often heterogeneous in tumors), and can also be used for diagnosis [6].

Several ultrasound imaging modes have been explored for angiogenesis imaging. Contrast-enhanced Doppler is unable to image tumor microcirculation due to a resolution limit of approximately 100 μm [14] and the tendency of contrast to create large “blooming artifacts” [15] but the contrast signal has been shown to correlate best to vessels of 20–39 μm in diameter [16]. Pulse inversion harmonic imaging (HI) is now a well established contrast imaging mode which suppresses linear tissue harmonic signals while improving the detection of nonlinear harmonics generated by UCA; and this imaging mode has been shown to improve the visualization of tumor microcirculation [1, 17]. Additionally, the use of destruction/ replenishment pulse sequences has been shown to increase the ability to visualize microcirculation and perfusion [18–20]. Microflow imaging (MFI) is one such emerging contrast imaging mode based on UCA destructive pulses followed by lower intensity imaging to generate cumulative maximum intensity images of microvasculature [18–20].

While CEUS has been shown to be useful for monitoring angiogenesis, results of correlating lesion vascularity with immunohistochemical markers have been mixed [21–23]. Previously, we compared UCA-derived fractional vascularity measurements with four immunohistochemical markers of angiogenesis in two murine xenograft tumor models using 4 ultrasound imaging modes (power Doppler, HI, MFI, and flash echo imaging). Results varied with imaging mode, marker, and tumor model, but showed correlations ranging from 0.00 to 0.41 [23]. While these results are encouraging, it is hypothesized that UCA wash-in derived blood flow parameters may more strongly correlate with immunohistochemical

NIH-PA Author Manuscript

NIH-PA Author Manuscript

NIH-PA Author Manuscript

markers of angiogenesis than fractional vascularity measures from a single time point. In this manuscript we explore parametric analysis of this dataset to strengthen these correlations through the incorporation of temporal information.

2. Materials and Methods

2.1 Ultrasound Imaging and pathology

All animal studies were performed under the guidance of a licensed veterinarian and all protocols were approved by Thomas Jefferson University's Institutional Animal Care and Use committee. Ultrasound imaging and pathology were originally obtained as part of a previous study comparing single time point based fractional vascularity measurements with immunohistochemical markers and has already been described in detail [23]. Briefly, 144 female 200–250 g, Sprague Dawly rats (Taconic Inc., Hudson, NY) were implanted with either C6 glioma cells or NMU mammary gland adenocarcinoma cells (ATTC, Manassas VA). Approximately 2E6 cells were injected subcutaneously into either the thigh or abdomen. Rats were then imaged and sacrificed at either 6, 8, or 10 days post implantation with 12 randomly assigned rats per group (3 time points × 2 implant location × 2 cell lines).

Prior to imaging, rats were anesthetized and a tail vein catheterized using a 24-gauge needle. Ultrasound imaging was performed using power Doppler imaging (PDI), pulse inversion harmonic imaging (HI), and microflow imaging (MFI) on an Aplio scanner with a 7.5 MHz linear array (Toshiba America Medical Systems, Tustin, CA). Ultrasound imaging was performed during bolus tail vein injection of the UCA Optison (GE Healthcare, Princeton, NJ; 0.4 ml/kg for each imaging mode). Contrast wash-in and wash-out were observed and cine loops stored for post processing. Injections were spaced out 3 to 5 minutes to avoid imaging of residual contrast.

Immediately after scanning, animals were sacrificed and the tumors excised. *Ex vivo* scanning was performed to identify the appropriate scan plane. Tumors were fixed in 10% formalin phosphate (Fisher Scientific, Houston, TX) for 12–24 hours before being washed and fixed in paraffin. Tumor slices were then stained for Cyclooxygenase-2 (COX2; using a monoclonal antibody from Santa Cruz Biotechnology, Santa Cruz CA), platelet endothelial cell adhesion molecules (using a monoclonal CD31 antibody; Dako Corporation, Carpinteria, CA), basic fibroblast growth factor (bFGF; using a polyclonal antibody from Santa Cruz Biotechnology, Santa Cruz, CA), and vascular endothelial growth factor (VEGF; using a monoclonal antibody from Oncogene Research Products, San Diego, CA). Finally, stained tissue slices were mounted on glass slides and immunohistochemical markers quantified using a semi-automated histomorphology setup as previously described [23].

2.2 Derivation of blood flow parameters

Stored video data from PDI, HI, and MFI exams from each rat were loaded in Matlab (Version 2012a; The Mathworks Inc, Natick MA) for processing. All parametric analysis was performed while blinded to histological results. Because analysis was done on a pixel-by-pixel basis, five rats from the C6 group and four from the NMU were removed due to excessive motion in at least one contrast exam. Time intensity curves were then generated for each individual pixel within the imaging window from the time of contrast injection to peak enhancement. Briefly, this parametric algorithm calculates the signal intensity over time for each pixel to create a time intensity versus intensity curve. These curves typically show a stable baseline intensity level, followed by a sharp rise in intensity at contrast arrival, followed by a gradual decrease in signal intensity as the UCA washes out of the tumor vasculature. From this information parametric maps displaying a maximum intensity projection (MIP; identified as peak pixel intensity in arbitrary units), the time to peak (TTP;

NIH-PA Author Manuscript

NIH-PA Author Manuscript

NIH-PA Author Manuscript

the time taken from injection to reach peak intensity in seconds), perfusion (PER; defined as MIP/TTP), and time integrated intensity (TII; defined as the area under the time intensity curve from contrast injection to peak enhancement) were calculated for each exam.

An unprocessed image from each video at baseline (prior to contrast arrival) was used to select as large a rectangular area as possible from within the tumor border. While a circular region of interest may have better encompassed the tumor area, it would also be more susceptible to sampling outside the tumor area at the occurrence of motion. Coordinates from this selection were then applied to the four parametric maps and the pixels within the border averaged to derive the four blood flow parameters for the entire tumor area. These four parameters from each imaging mode were then matched to the immunohistochemical findings quantified as part of our previously reported study [23].

2.3 Statistical Analysis

All statistical analyses were performed in GraphPad Prism (Version 5.0, GraphPad Software, San Diego CA). Pearson coefficients (R; the standard measure of strength in correlation between two groups of variables) were computed to calculate the linear correlation of each temporal parameter to each immunohistochemical marker. Bonferroni correction of 16 multiple comparisons (from the 4 × 4 datasets, used to avoid errors of perceived significance by chance while performing multiple comparison) was used with statistical significance determined by $p < 0.05$ [24]. For the sake of discussion purposes, strong correlation was classified as having an absolute value correlation greater than 0.35, while weak correlation was classified as an absolute value less than 0.15. Analysis was first performed over the entire dataset (133 rats). Analysis was then repeated subgrouping the data by both type (C6 and NMU separately) or by location (thigh and abdomen implanted tumors separately).

3. Results

Data was excluded from five C6 rats and four NMU rats due to excessive motion during scanning. Parametric maps showing maximum intensity projections (MIP), time to peak from contrast injection (TTP), perfusion (PER), and time-integrated intensity (TII) were successfully generated for the remaining rats. Figure 1 shows example images of baseline and peak enhancements images of a C6 tumor implanted in the thigh during contrast-enhanced ultrasound scanning by PDI (a–b), HI (c–d), and MFI (e–f) with the tumor circled at baseline. Figure 2 shows the corresponding parametric maps generated from the HI mode of the case shown in Fig 1 (a: MIP, b: TTP, c: Per, d: TII).Within the tumor, these maps present temporal information on the degree of vascularity, resistance to flow, rate of blood flow, and a cumulative blood transport. In this example, the boundary of the tumor is well defined for all cases, with MIP and TTP also showing the vascular area of the mass (bottom left quadrant).

After generating individual parametric maps for each tumor, values over the tumor areas were averaged to get an overall indicator of blood flow kinetics for the tumor as a whole and compared to angiogenesis markers. Table 21 shows the entire data set correlation of these parameters from each imaging mode with the four investigated angiogenic markers with statistically significant correlations marked in bold. Within all temporal parameters and angiogenic markers, a statistically significant correlation was only observed between VEGF expression and TII. This negative correlation was consistent among all three imaging modes, with HI resulting in the strongest correlation of $R = -0.54$. While much of TII values are relatively low, a gradual decrease is observed with increasing VEGF expression in each of the three modes. Data from these correlations are shown in Figure 3.

NIH-PA Author Manuscript

NIH-PA Author Manuscript

NIH-PA Author Manuscript

To explore the effects of tumor model on these correlations, analysis was then split into tumor subgroups. Correlations are shown in Tables 2–3. When looking only within the C6 subgroup (Table 2), correlations between VEGF and TII remain consistent with strong inverse correlation among all three imaging modes. HI again results in a correlation of R= −0.54, but correlations between TII and VEGF increase for both the PDI (−0.43) and MFI (−0.52). Additionally, strong negative correlations are also observed between TTP and the angiogenesis markers COX2 and bFGF. Interestingly, when looking the NMU subgroup (Table 4) all correlations between TII and VEGF remain negative, but become non-significant, presumably due to increased variability in the NMU group.

Similar to the approach used for grouping results by tumor model, Tables 4–5 show the correlation of all immunohistochemical markers with temporal parameters when grouping the dataset by implant location. Consistent with correlations from the entire dataset, abdomen data (Table 4) showed strong negative correlation between TII and VEGF for all three imaging modes. Correlation improved to −0.41 for PDI, −0.58 for HI and −0.38 for MFI. Table 5 shows that correlations of TII with VEGF from thigh implanted data alone decreased relative to the cumulative dataset for each of the imaging modes.

4. Discussion

Results from this study indicate blood flow parameters derived from ultrasound contrast agents may be a good overall indicator of angiogenic markers, although these correlations are both tumor and imaging mode dependant. Results among imaging modes suggest an adequate ability to visualize the tumor vascularity in real time is important. As can be seen in Figure 1b PDI's high sensitivity (relative to HI or MFI) to contrast results in signal covering the entire tumor area and margins. This artifact, termed blooming restricts the ability to view tumor microcirculation, due to saturation of the interrogated area [15]. Contrast-enhanced HI (Fig 1d) does not suffer from this artifact and gives better indication of vascular regions within the tumor. Microflow imaging provides improved visualization of microvessels during contrast wash in, but the cumulative maximum intensity nature is also more prone to blurring artifacts over time as peak intensity is reached as can been seen in Fig 1f. As a result, stronger correlations were detected using HI and are attributed to the mode being the best overall compromise of microvascular resolution while still avoiding temporal artifacts generated by flash-replenishment and cumulative maximum intensity techniques in MFI.

Parametric imaging has been used extensively in CEUS, primarily for lesion characterization [6, 8, 24–26]. Often curve fitting is applied for contrast wash in/wash out over the entire mass volume as this has been shown to reduce intra- and inter-reader variability [26–28]. Generation of parametric maps on a pixel basis results in a higher level of detail within a heterogeneous tumor volume (as shown in Figure 2), but curve fitting is not applicable for changes over such as small area. However, this pixel by pixel approach may also not be feasible for deeper tissue imaging due to motion artifacts.

Previously, when examining this data set we compared single time point, fractional vascularity measurements to all 4 immunohistochemical markers and found strongest correlations to VEGF using HI [23]. However these correlations were subgroup dependent and only R = 0.24, 0.21, 0.17, and 0.34 within the C6 (glioma cell line) abdomen implanted, C6 thigh implanted, NMU (breast cancer cell line) abdomen implanted, and NMU thigh implanted subgroups respectively [23]. Correlations from Table 1 show that a stronger (R= −0.54 vs. R < 0.46 when broken down into 1 implant/location and no significant trends over the entire dataset in [23]), more robust correlation to VEGF can be achieved when incorporating temporal information using parametric imaging. Recently, Zhuang and

NIH-PA Author Manuscript

NIH-PA Author Manuscript

NIH-PA Author Manuscript

colleagues used UCA time intensity curve analysis in 39 patients with colorectal tumors [29]. The group found a strong correlation between TII and tumor microvessel density (R = 0.69), but no significant correlations with VEGF expression. This difference in findings is likely due to the degree of physiological variability in a human clinical population versus a controlled tumor model in rats. Thus, the work presented in this study may not be practical as a screening tool in human populations, but may be useful as a drug pipeline screening tool in more controlled animal models or as a potential response monitoring tool in humans by following the same patient over time (thus decreasing the variability).

Tables 2–5 show that correlations of the contrast derived flow parameters with angiogenic markers are both tumor type and implant location dependant. When comparing table 2 with table 3, we see stronger overall correlation with contrast derived parameters in C6 tumors relative to NMU. While TII's correlation to VEGF remained the strongest for both subgroup, variations in the strength of correlations between the two tumor types is attributed to biological variability. When investigating correlations on a implant location-based approach, correlations further improved when only examining tumors implanted in the abdomen region (Table 4). These improvements are somewhat expected in that UCA was injected via tail vein and a single implant location will help to standardize time intensity curves by providing a more consistent UCA transit time from injection to tumor arrival. Interesting, table 5 shows that correlations of TII with VEGF from thigh implanted data alone decreased relative to the cumulative dataset for each of the imaging modes (Table 1). While the reasoning of this drop in correlation is not yet understood, it demonstrates that implant location is also important when using dynamic CEUS for estimating angiogenesis markers in a tumor model.

Several groups have used CEUS for the early identification of anti-angiogenic therapy [30–32]. However, while this work has investigated some temporal changes such as perfusion, these correlations have almost entirely focused on changes in tumor volume, whereas changes in angiogenic biomarkers may be a more suitable marker of treatment response in anti-angiogenic therapy. Another emerging application in anti-angiogenic therapy monitoring is the use of targeted UCA, which employ targeting ligands on their surface [33,34]. These microbubbles have been tailored to bind to VEGF among other vascularly expressed receptors and may offer a substantial improvement for therapy monitoring [35]. However these agents are not currently approved for clinical use and are costly for research purposes. Thus, parametric imaging of dynamic CEUS may be a useful alternative as an inexpensive (roughly 10–20% in cost of either an X-ray computed tomography or magnetic resonance imaging exam), reliable estimate of VEGF in tumor models.

Despite being the largest study to our knowledge comparing parametric CEUS with immunohistochemical markers, several limitations exist in this study. As can be seen in Figure 3, a large percentage of the TII data appears to approach zero across the entire range of VEGF expression. However, while thresholding may alleviate some of these issues in the future, a strong, statistically significant correlation was still detected. Additionally, the thickness of the ultrasound beam (on the mm scale) is significantly larger than the tissue slices obtained for histology (on the μm scale), and while great care was taken to match images to the corresponding tissue slice, some discrepancy in location may still exist between pathology and imaging plane. Finally, imaging was performed in the near field with a clinical scanner designed for deeper scanning (and beyond the depth of a standoff pad) and the use of a higher-frequency small-animal scanner may potentially improve contrast visualization and ultimately strengthen these correlations.

NIH-PA Author Manuscript

NIH-PA Author Manuscript

NIH-PA Author Manuscript

5. Conclusions

Time-integrated intensity of UCA wash-in appears to correlate well with VEGF expression in two murine xenografts for each investigated imaging mode. While correlations were found to depend on both tumor type and implant location, correlations are stronger than those previously reported using fractional vascularity estimates from single time points. Thus, the incorporation of temporal information with parametric imaging may provide a more robust measure of the tumor microenvironment and may be useful for future anti-angiogenic drug screening.

Acknowledgments

This work was supported by NIH CA093907 and US Army Medical Research Material Command Grant W81XWH-11-1-0630 (JRE). The contrast agent was provided by GE Healthcare, Princeton, NJ, while Toshiba America Medical Systems, Tustin, CA provided the ultrasound scanner.

References

1. Goldberg, BB.; Raichlen, JS.; Forsberg, F. Ultrasound Contrast Agents: Basic Principles and Clinical Applications. second ed.. London, England: Martin Dunitz Ltd; 2001.
2. Greis C. Ultrasound contrast agents as markers of vascularity and microcirculation. Clin. Hemorheol. Microcirc. 2009; 43:1–9. [PubMed: 19713597]
3. Hudson JM, Karshafian R, Burns PN. Quantification of flow using ultrasound and microbubbles: a disruption replenishment model based on physical principles. Ultrasound Med. Biol. 2009; 35:2007–2020. [PubMed: 19822390]
4. Feingold S, Gessner R, Guracar IM, et al. Quantitative volumetric perfusion mapping of the microvasculature using contrast ultrasound. Invest.Radiol. 2010; 45:669–674. [PubMed: 20808232]
5. Kogan P, Johnson KA, Feingold S, et al. Validation of dynamic contrast-enhanced ultrasound in rodent kidneys as an absolute quantitative method for measuring blood perfusion. Ultrasound Med. Biol. 2011; 37:900–908. [PubMed: 21601135]
6. Eisenbrey JR, Dave JK, Merton DA, et al. Parametric imaging using subharmonic signals from ultrasound contrast agents in patients with breast lesions. J. Ultrasound Med. 2011; 30:85–92. [PubMed: 21193708]
7. Pollard RE, Broumas AR, Wisner ER, et al. Quantitative contrast enhanced ultrasound and CT assessment of tumor response to antiangiogenic therapy in rats. Ultrasound Med. Biol. 2007; 33:235–245. [PubMed: 17306694]
8. Lassau N, Koscielny S, Albiges L, et al. Metastatic renal cell carcinoma treated with sunitinib: early evaluation of treatment response using dynamic contrast enhanced ultrasonography. Clin. Cancer Res. 2010; 16:1216–1225. [PubMed: 20145174]
9. Guibal A, Taillade L, Mulé S, et al. Noninvasive contrast-enhanced US quantitative assessment of tumor microcirculation in a murine model: effect of discontinuing anti-VEGF therapy. Radiology. 2010; 254:420–429. [PubMed: 20093514]
10. Eisenbrey JR, Forsberg F. Contrast-enhanced ultrasound for molecular imaging of angiogenesis. Eur. J. Nucl. Med. Mol. Imaging. 2010; 37:S138–S146. [PubMed: 20461376]
11. Averkiou M, Lampaskis M, Kyriakopoulou K, et al. Quantification of tumor microvascularity with respiratory gated contrast enhanced ultrasound for monitoring therapy. Ultrasound Med. Biol. 2010; 36:68–77. [PubMed: 19900749]
12. Leong-Poi H. Molecular imaging using contrast-enhanced ultrasound: evaluation of angiogenesis and cell therapy. Cardiovasc. Res. 2009; 84:190–200. [PubMed: 19628466]
13. Cosgrove D, Lassua N. Imaging of perfusion using ultrasound. Eur. J. Nucl. Med. Mol. Imaging. 2010; 37:S65–S85. [PubMed: 20640418]
14. Ferrara KF, Merritt CRB, Burns PN. Evaluation of tumor angiogenesis with US: imaging, Doppler and contrast agents. Acad. Radiol. 2000; 7:824–839. [PubMed: 11048880]

NIH-PA Author Manuscript

NIH-PA Author Manuscript

NIH-PA Author Manuscript

15. Forsberg F, Liu JB, Burns PN, et al. Artifacts in ultrasonic contrast agent studies. J. Ultrasound Med. 1994; 13:357–365. [PubMed: 8015042]
16. Forsberg F, Kuruvilla B, Pascua MB, et al. Comparing contrast-enhanced color flow imaging andpathological measures of breast lesion vascularity. Ultrasound Med. Biol. 2008; 34:1365–1372. [PubMed: 18436369]
17. Jung EM, Kubale R, Jungius KP, et al. Vascularization of liver tumors- preliminary results with coded harmonic angio (CHA), phase inversion imaging, 3D power Doppler and contrast medium-enhanced B-flow with second generation contrast agent (Optison). Clin. Hemorheol. Microcirc. 2006; 34:483–497. [PubMed: 16687788]
18. Linden RA, Trabulsi EJ, Forsberg F, et al. Contrast enhanced ultrasound flash replenishment method for directed prostate biopsies. J. Urol. 2007; 178:2354–2359. [PubMed: 17936814]
19. Sugimoto K, Moriyasu F, Kamiyama N, et al. Analysis of morphological vascular changes of hepatocellular carcinoma by microflow imaging using contrast-enhanced sonography. Hepatol. Res. 2008; 38:790–797. [PubMed: 18507694]
20. Wilson SR, Jang HY, Kim TK, et al. Real-time temporal maximum-intensity-projection imaging of hepatic lesions with contrast-enhanced sonography. AJR Am. J. Roentgenol. 2008; 190:691–695. [PubMed: 18287440]
21. Forsberg F, Dicker AP, Thakur ML, et al. Comparing contrast-enhanced ultrasound to immunohistochemical markers of angiogenesis in a human melanoma xenograft model: preliminary results. Ultrasound Med. Biol. 2002; 28:445–451. [PubMed: 12049957]
22. Du J, Li FH, Fang H, et al. Correlation of real-time gray scale contrast-enhanced ultrasonography with microvessel density and vascular endothelial growth factor expression for assessment of angiogenesis in breast lesions. J. Ultrasound Med. 2008; 27:821–831. [PubMed: 18499842]
23. Forsberg F, Ro RJ, Fox TB, et al. Contrast enhanced maximum intensity projection ultrasound imaging for assessing angiogenesis in murine glioma and breast tumor models: a comparative study. Ultrasonics. 2011; 51:382–389. [PubMed: 21144542]
24. Rosner, B. Fundamentals of biostatistics. 7th Ed.. Boston, MA: Brooks/Cole; 2011.
25. Wakui N, Takayama R, Kamiyama N, et al. Diagnosis of hepatic hemangioma by parametric imaging using sonzaoid-enhanced US. Hepatogastroenterology. 2011; 58:1431–1435. [PubMed: 21940325]
26. Zhao H, Xu R, Ouyang Q, et al. Contrast-enhanced ultrasound is helpful in the differentiation of malignant and benign breast lesions. Eur. J. Radiol. 2010; 73:288–293. [PubMed: 19559551]
27. Dietrich CF, Averkious MA, Correas JM, et al. An EFSUMB introduction into dynamic contrast enhanced ultrasound (DCE-US) for quantification of tumor perfusion. Ultraschall.Med. 2012; 33:344–351. [PubMed: 22843433]
28. Gauthier TP, Muhammad A, Wasan HS, et al. Reproducibility of quantitative assessment of altered hepatic hemodynamics with dynamic contrast-enhanced ultrasound. J. Ultrasound Med. 2012; 31:1413–1420. [PubMed: 22922621]
29. Gauthier M, Tabarout F, Leguerney I, et al. Assessment of quantitative parameters by dynamic contrast-enhanced sonography using a deconvolution method: an in vitro and in vivo study. J. Ultrasound Med. 2012; 52:12–19.
30. Zhuang H, Yang ZG, Chen HG, et al. Time-intensity curve parameters in colorectal tumours measured using double-contrast-enhanced ultrasound: correlations with tumor angiogenesis. Colorectal. Dis. 2012; 14:181–187. [PubMed: 21689263]
31. Hoyt K, Warram JM, Umphrey H, et al. Determination of breast cancer response to bevacizumab therapy using contrast-enhanced ultrasound and artificial neural networks. J. Ultrasound Med. 2010; 29:577–585. [PubMed: 20375376]
32. Lassau N, Lamuraglia M, Chami L, et al. Gastrointesitinal stromal tumors treated with imatinib: monitoring treatment response with contrast-enhanced sonography. AJR Am J. Roentgenol. 2006; 187:1267–1273. [PubMed: 17056915]
33. Williams R, Hudson JM, Lloyd BA, et al. Dynamic microbubble contrast-enhanced US to measure tumor response to targeted therapy: a proposed clinical protocol with results from renal cell carcinoma patients receiving antiangiogenic therapy. Radiology. 2011; 260:581–590. [PubMed: 21555352]

NIH-PA Author Manuscript
NIH-PA Author Manuscript
NIH-PA Author Manuscript

34. Siri S, Flexman ML, Vlachos F, et al. Contrast ultrasound imaging for identification of early responder tumor models to anti-angiogenic therapy. Ultrasound Med. Biol. 2012; 38:1019–1029. [PubMed: 22425376]

35. Pysz MA, Foygel K, Rosenberg J, et al. Antiangiogenic cancer therapy: monitoring with molecular US and a clinically translatable contrast agent (BR55). Radiology. 2010; 256:519–527. [PubMed: 20515975]

36. Klibanov A. Microbubble contrast agents: targeted ultrasound imaging and ultrasound- assisted drug delivery applications. Invest. Radiol. 2006; 41:354–362. [PubMed: 16481920]

Appendix 1

Appendix 1

Abbreviations used throughout text

Abbreviation	Term
bFGF	Basic fibroblast growth factor
CD31	An antibody for platelet endothelial cell adhesion molecules
Cox 2	Cyclooxygenase-2
CEUS	Contrast enhanced ultrasound
HI	Harmonic Imaging
MFI	Microflow Imaging
MIP	Maximum Intensity Projection
PDI	Power Doppler Imaging
PER	Perfusion (arbitrary units / second)
TII	Time integrated intensity (arbitrary units × seconds)
TTP	Time to peak (seconds)
UCA	Ultrasound contrast agent
VEGF	Vascular endothelial growth factor

NIH-PA Author Manuscript

NIH-PA Author Manuscript

NIH-PA Author Manuscript

Study Highlights

- Ultrasound contrast kinetics were compared to angiogenesis markers
- Three contrast imaging modes were compared with four markers
- Strongest correlation was observed between harmonic imaging and VEGF expression
- These correlations were stronger than previous fractional vascularity measurements
- Strength of correlation depended on both tumor type and implant location

-include 3 to 5 bullet points (maximum 85 characters, including spaces, per bullet point).

NIH-PA Author Manuscript
NIH-PA Author Manuscript
NIH-PA Author Manuscript

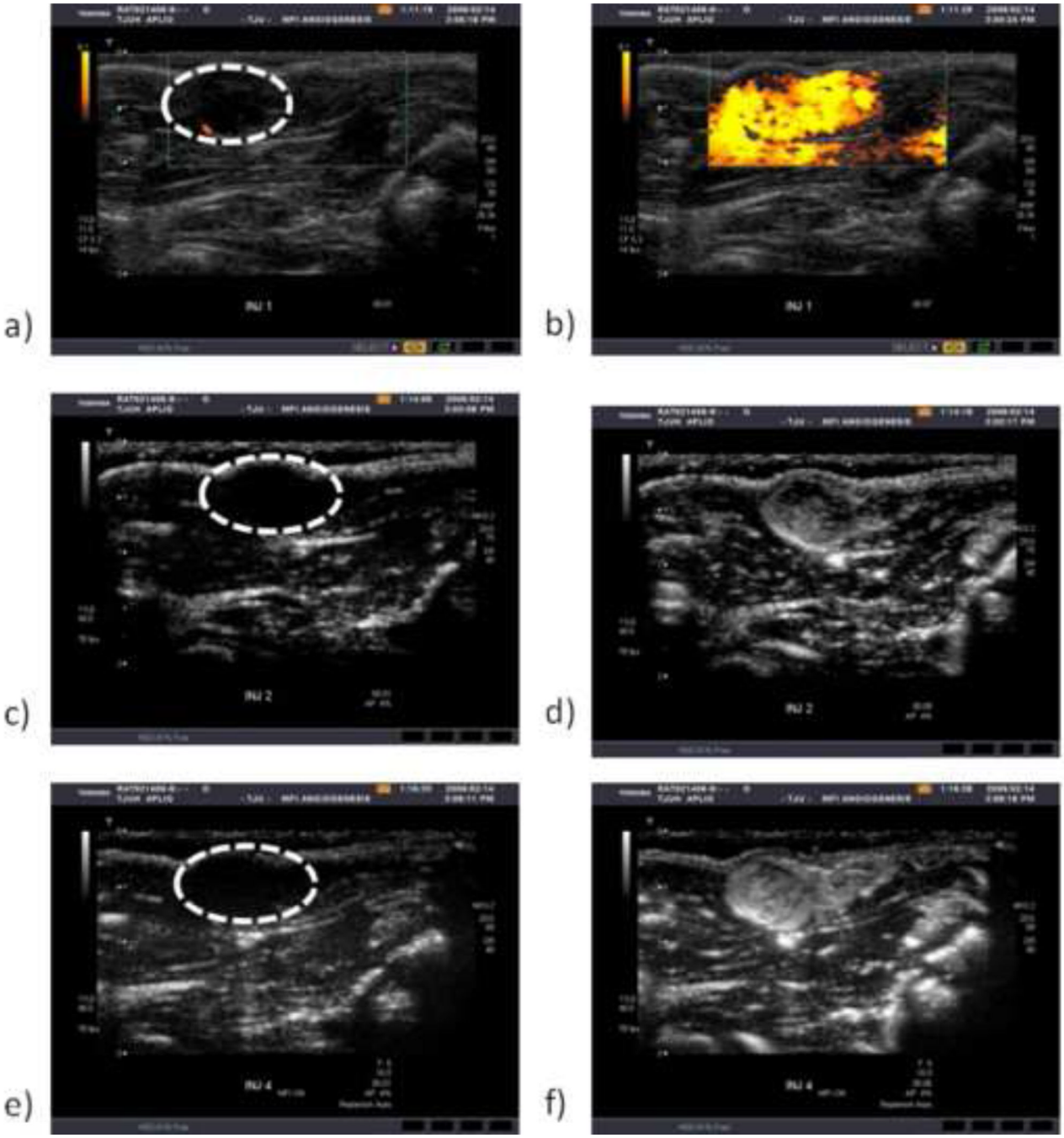

Figure 1.
Example images showing baseline (with tumor circled) and peak enhancement of a C6 thigh implanted tumor imaged with PDI (a–b), HI (c–d), and MFI (e–f).

NIH-PA Author Manuscript
NIH-PA Author Manuscript
NIH-PA Author Manuscript

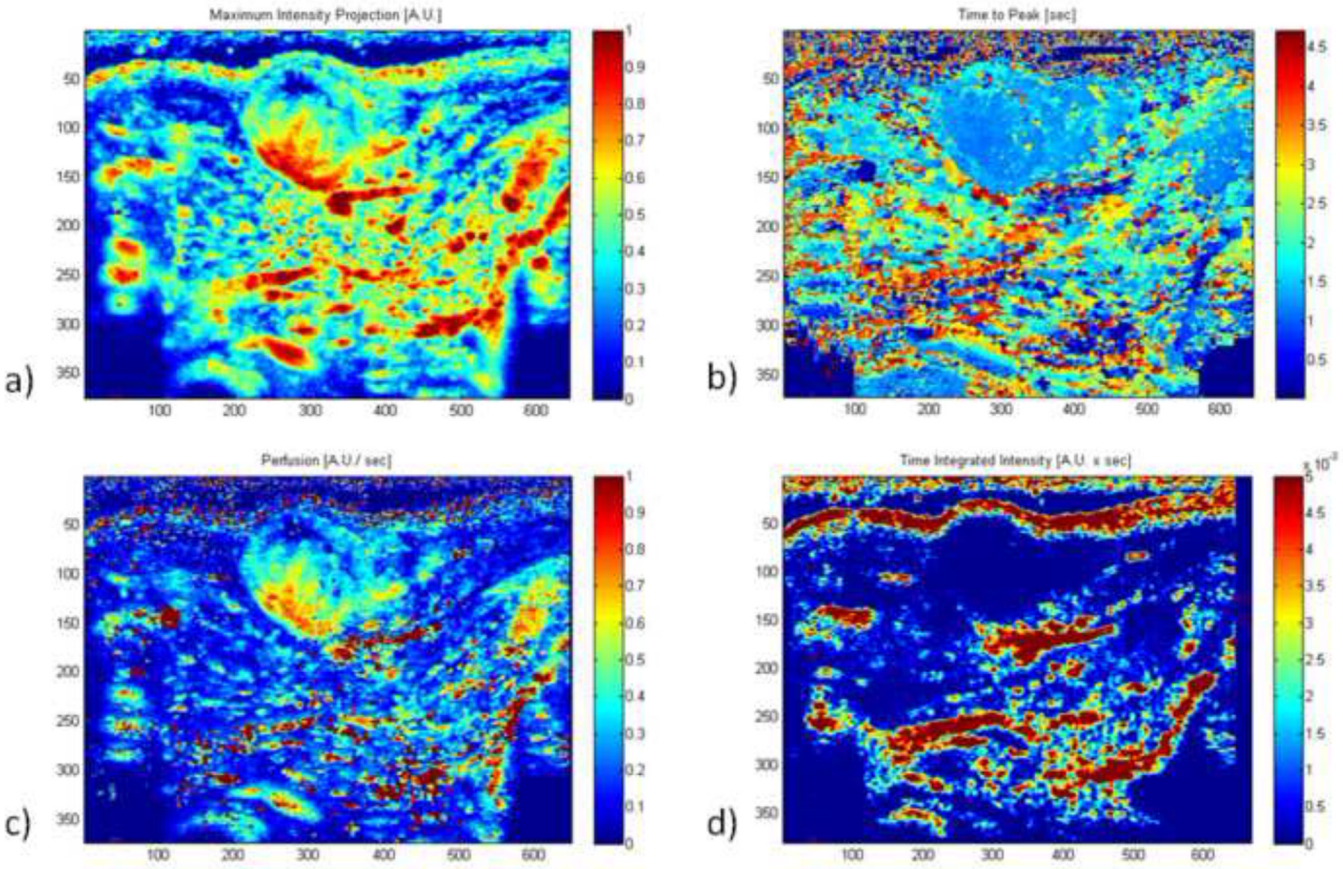

Figure 2.

Example parametric images generated from the harmonic case in Figure 1, showing maximum intensity (a), time to peak (b), perfusion (c), and time integrated intensity (d) (A.U. = arbitrary units).

NIH-PA Author Manuscript
NIH-PA Author Manuscript
NIH-PA Author Manuscript

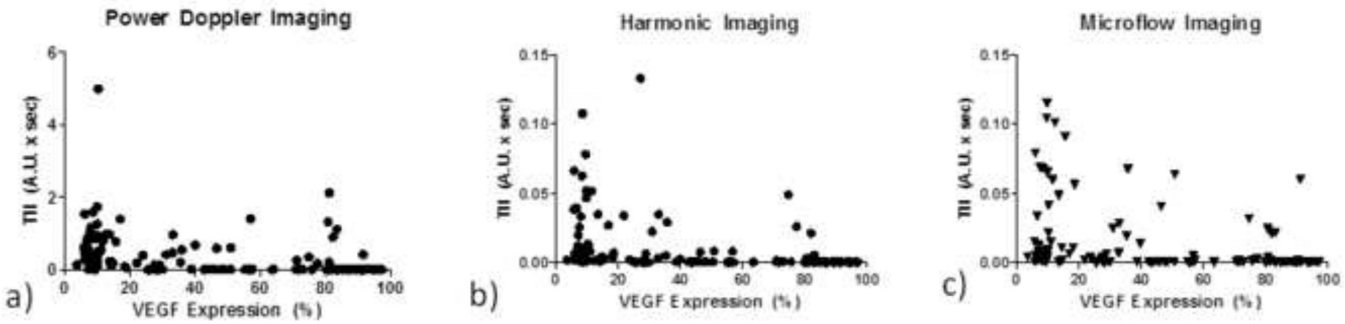

Figure 3.

Data from correlation of time integrated intensity (TII) with vascular endothelial growth factor (VEGF) expression from power Doppler (a), harmonic (b), and microflow (c) imaging.

NIH-PA Author Manuscript
NIH-PA Author Manuscript
NIH-PA Author Manuscript

Table 1

Correlation of all parametric data points to corresponding immunohistochemical markers

	Power Doppler				Harmonic Imaging				Microflow Imaging			
	MIP	**TTP**	**PER**	**TII**	**MIP**	**TTP**	**PER**	**TII**	**MIP**	**TTP**	**PER**	**TII**
bFGF	0.10	−0.16	0.05	0.12	0.04	0.14	0.05	0.04	0.06	−0.24	0.16	0.17
CD31	0.03	−0.11	0.06	0.03	0.03	0.00	0.00	0.03	−0.09	0.04	−0.09	0.14
Cox-2	0.14	−0.12	0.09	0.20	0.09	−0.12	0.16	0.13	0.14	−0.13	0.17	0.19
VEGF	−0.04	0.24	−0.15	**−0.35**	−0.20	0.10	−0.30	**−0.54**	0.13	0.17	0.04	**−0.32**

*Statistically significant correlations bolded; $p < 0.05$.

NIH-PA Author Manuscript
NIH-PA Author Manuscript
NIH-PA Author Manuscript

Table 2

Correlation of all C6 tumor parametric data points to corresponding immunohistochemical markers

	Power Doppler				Harmonic Imaging				Microflow Imaging			
	MIP	**TTP**	**PER**	**TII**	**MIP**	**TTP**	**PER**	**TII**	**MIP**	**TTP**	**PER**	**TII**
bFGF	0.00	−0.26	0.06	0.09	−0.18	−0.31	−0.07	0.11	0.04	**−0.48**	0.16	0.17
CD31	−0.09	−0.19	0.05	0.11	−0.06	−0.17	−0.02	0.10	−0.03	−0.22	−0.02	0.31
Cox-2	0.07	−0.15	0.09	0.22	−0.10	−0.34	0.06	0.18	0.06	**−0.37**	0.11	0.29
VEGF	−0.17	0.28	−0.25	**−0.43**	−0.20	0.10	−0.30	**−0.54**	0.04	0.26	−.14	0.52

*Statistically significant correlations bolded; $p < 0.05$.

NIH-PA Author Manuscript
NIH-PA Author Manuscript
NIH-PA Author Manuscript

Table 3

Correlation of all NMU tumor parametric data points to corresponding immunohistochemical markers

	Power Doppler				Harmonic Imaging				Microflow Imaging			
	MIP	**TTP**	**PER**	**TII**	**MIP**	**TTP**	**PER**	**TII**	**MIP**	**TTP**	**PER**	**TII**
bFGF	0.12	−0.09	0.07	0.13	0.17	0.06	0.16	0.11	0.17	0.05	0.17	0.07
CD31	0.12	−0.04	0.06	−0.10	0.10	0.10	0.03	−0.01	−0.14	0.13	−0.13	−0.09
Cox-2	0.19	−0.09	0.10	0.17	0.28	0.04	0.23	0.11	0.21	0.03	0.21	0.05
VEGF	0.09	0.24	−0.08	−0.32	−0.12	0.24	−0.18	−0.21	0.30	0.30	0.17	−0.14

*Statistically significant correlations bolded; $p < 0.05$.

NIH-PA Author Manuscript
NIH-PA Author Manuscript
NIH-PA Author Manuscript

Table 4

Correlation of all abdomen-implanted tumor parametric data points to corresponding immunohistochemical markers

	Power Doppler				Harmonic Imaging				Microflow Imaging			
	MIP	**TTP**	**PER**	**TII**	**MIP**	**TTP**	**PER**	**TII**	**MIP**	**TTP**	**PER**	**TII**
bFGF	0.09	−0.29	0.31	0.11	0.21	−0.08	0.15	0.12	−0.13	−0.30	0.15	0.25
CD31	0.05	−0.19	0.19	0.00	0.15	0.01	0.04	0.01	0.07	0.06	−0.05	0.18
Cox-2	0.12	−0.03	0.14	0.10	0.04	0.13	0.02	0.07	−0.03	−0.03	−0.06	0.16
VEGF	−0.17	**0.40**	−0.25	**−0.41**	−0.22	0.38	−0.40	**−0.55**	0.05	0.30	−0.10	**−0.38**

*Statistically significant correlations bolded; $p < 0.05$.

NIH-PA Author Manuscript
NIH-PA Author Manuscript
NIH-PA Author Manuscript

Table 5

Correlation of all thigh-implanted tumor parametric data points to corresponding immunohistochemical markers

	Power Doppler				Harmonic Imaging				Microflow Imaging			
	MIP	**TTP**	**PER**	**TII**	**MIP**	**TTP**	**PER**	**TII**	**MIP**	**TTP**	**PER**	**TII**
bFGF	0.08	0.04	−0.15	0.12	−0.17	−0.22	−0.07	−0.06	0.20	−0.17	0.18	0.08
CD31	0.02	−0.2	−0.01	0.09	−0.14	−0.07	−0.01	0.06	−0.23	−0.02	−0.12	0.06
Cox-2	0.12	−0.18	0.02	**0.37**	0.14	**−0.46**	0.31	0.22	0.27	−0.23	0.32	0.26
VEGF	0.00	0.26	−0.24	−0.28	−0.31	0.22	**−0.40**	**−0.45**	0.14	0.14	0.08	−0.21

*Statistically significant correlations bolded; $p < 0.05$.